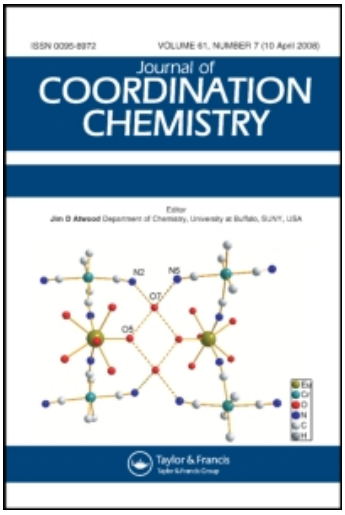

Journal of Coordination Chemistry
Publication details, including instructions for authors and subscription information:
http://www.informaworld.com/smpp/title~content=t713455674

Co(II) halide complexes with 2-amino-3-methylpyridinium and 2-amino-5-methylpyridinium: synthesis, crystal structures, and magnetic properties

David J. Carnevale[a]; Christopher P. Landee[b]; Mark M. Turnbull[a]; Mon Winn[a]; Fan Xiao[b]
[a] Carlson School of Chemistry and Biochemistry, Clark University, Worcester, MA 01610, USA [b] Department of Physics, Clark University, Worcester, MA 01610, USA

First published on: 14 July 2010

To cite this Article Carnevale, David J. , Landee, Christopher P. , Turnbull, Mark M. , Winn, Mon and Xiao, Fan(2010) 'Co(II) halide complexes with 2-amino-3-methylpyridinium and 2-amino-5-methylpyridinium: synthesis, crystal structures, and magnetic properties', Journal of Coordination Chemistry, 63: 13, 2223 — 2238, First published on: 14 July 2010 (iFirst)
To link to this Article: DOI: 10.1080/00958972.2010.502230
URL: http://dx.doi.org/10.1080/00958972.2010.502230

Journal of Coordination Chemistry
Vol. 63, No. 13, 10 July 2010, 2223–2238

Co(II) halide complexes with 2-amino-3-methylpyridinium and 2-amino-5-methylpyridinium: synthesis, crystal structures, and magnetic properties

DAVID J. CARNEVALE†, CHRISTOPHER P. LANDEE‡, MARK M. TURNBULL*†, MON WINN† and FAN XIAO‡

†Carlson School of Chemistry and Biochemistry, Clark University, Worcester, MA 01610, USA
‡Department of Physics, Clark University, Worcester, MA 01610, USA

(*Received 12 March 2010; in final form 5 May 2010*)

Reaction of $CoX_2 \cdot nH_2O$ with either 2-amino-3-methylpyridine (3-MAP) or 2-amino-5-methylpyridine (5-MAP) in aqueous acid gave complexes, $(3\text{-MAPH})_2CoX_4$ or $(5\text{-MAPH})_2CoX_4\ (H_2O)_n$ [$n = 0,1$; X = Cl, Br; 3-MAPH = 2-amino-3-methylpyridinium, 5-MAPH = 2-amino-5-methylpyridinium]. The 3-MAPH salts are formed in the triclinic crystal system while the 5-MAPH salts are formed in the monoclinic crystal system. Three of these compounds exhibit weak antiferromagnetic interactions along with varying degrees of single-ion anisotropy, however, **1** shows easy-plane anisotropy and exhibits a mixture of ferromagnetic and antiferromagnetic interactions.

Keywords: Co(II); Magnetism; X-ray structure; XY-anisotropy

1. Introduction

The ongoing study of low-dimensional magnetic lattices has led us to study a series of compounds of formula $A_2[MX_4]$ where A is an organic cation, usually a protonated base, M is a 2+ transition metal ion, and X is a halide (Cl, Br). A wide variety of these complexes, especially with Cu(II) are known where the A-group is a protonated alkyl amine [1], or heterocycle such as pyridine [2], morpholine [3], or 2-aminopyrimidine [4]. The use of these nitrogen-based cations with their variety of size and shape produces chains, ladders, and sheets within the lattice, resulting in a variety of magnetic interactions. The magnetic properties of these compounds are dominated by van der Waals contacts between the halide of MX_4^{-2} (the two halide pathway [5]), and the contacts are determined by crystal packing.

The use of 2-amino-3-methylpyridine (3-MAP) and 2-amino-5-methylpyridine (5-MAP) allows us to study the effect of using cations of similar formula and molecular weight, but varying shape. The change in location of the methyl group on the 2-aminopyridine ring changes both the general shape (with the 2,5-substituted

*Corresponding author. Email: mturnbull@clarku.edu

Journal of Coordination Chemistry
ISSN 0095-8972 print/ISSN 1029-0389 online © 2010 Taylor & Francis
DOI: 10.1080/00958972.2010.502230

compound being more linear) and the hydrogen bonding capabilities (due to the change in proximity of the methyl group to the NH_2 substituent). A number of Cu(II) halide salts of these bases have been reported [6], including the A_2CuX_4 compounds [2, 7]. However, salts of other transition metals have been limited [8] and the only Co(II) containing structure reported is $(5\text{-MAPH})_2CoBr_4$ (5-MAPH = 2-amino-5-methylpyridinium), although no magnetic data were obtained [8c]. Changing the metal ion may affect the shape of MX_4^{2-} and as a result change both the structure of the crystal and the nature of the magnetic interactions in the crystal. This article reports the synthesis, structure, and magnetic properties of Co(II) chloride and bromide salts of 2-amino-3-methylpyridinium (3-MAP) and 2-amino-5-methylpyridinium (5-MAP).

2. Experimental

3-MAP and 5-MAP were purchased from Aldrich Chemical Corp. and used without purification. The transition metal halides were purchased from Alfa and used without purification. Infrared (IR) spectra were recorded on a Perkin Elmer 1600 FT-IR.

2.1. *Synthesis*

2.1.1. $(3\text{-MAPH})_2[CoBr_4]$ (1). A solution of 3-MAP (384.4 mg, 3.5 mmol) in 0.5 mL of aqueous HBr (3.56 mol L^{-1}, 1.78 mmol) was added to a solution of $CoBr_2 \cdot 4H_2O$ (365.5 mg, 1.25 mmol) in 1.0 mL of water. Dark blue crystals grew *via* slow evaporation and were collected *via* filtration after 2 weeks. Yield: 454 mg (61%) IR data (KBr, cm^{-1}): 3484 w, 3346 m, 3209 m, 3093 m, 1649 vs, 1623 sh, 1564 s, 1459 w, 1354 s, 1066 w, 784 m, 752 m, and 547 w.

2.1.2. $(5\text{-MAPH})_2[CoBr_4]$ (2). A solution of 5-MAP (511.8 mg, 4.7 mmol) in 1.0 mL of aqueous HBr (3.56 mol L^{-1}, 3.56 mmol) was added to a solution of $CoBr_2 \cdot 4H_2O$ (564.1 mg, 2.4 mmol) in 1.0 mL of water. Dark blue crystals grew *via* slow evaporation and were collected *via* filtration after 2 weeks. Yield: 377 mg (38%) IR data (KBr, cm^{-1}): 3298 m, 3183 m, 1666 vs, 1622 vs, 1550 m, 1462 w, 1348 w, 1320 w, 835 sh, 791 m, 759 sh, and 510 m.

2.1.3. $(3\text{-MAPH})_2[CoCl_4](H_2O)$ (3). A solution of 3-MAP (512.7 mg, 4.7 mmol) in 1.0 mL of aqueous HCl (12 mol L^{-1}, 12 mmol) was added to a solution of $CoCl_2 \cdot 6H_2O$ (563.3 mg, 2.4 mmol) in 1.0 mL of water. Blue crystals grew *via* slow evaporation and were collected *via* filtration after 2 weeks. Yield: 264 mg (26%) IR data (KBr, cm^{-1}): 3596 w, 3497 w, 3356 m, 3324 m, 3194 br, 1650 s, 1565 m, 1460 w, 1444 sh, 1356 w, 774 w, 758 sh, and 546 w.

2.1.4. $(5\text{-MAPH})_2[CoCl_4]$ (4). A solution of 5-MAP (361.7 mg, 3.3 mmol) in 0.5 mL of aqueous HCl (12 mol L^{-1}, 6 mmol) was added to a solution of $CoCl_2 \cdot 6H_2O$ (487.7 mg, 1.7 mmol) in 1.0 mL of water. Dark blue crystals grew *via* slow evaporation and were

collected *via* filtration after 2 weeks. Yield: 685 mg (69%) IR data (KBr, cm^{-1}): 3394 sh, 3311 m, 3186 m, 1669 vs, 1625 vs, 1552 w, 1465 w, 1353 w, 1322 w, 837 sh, 796 w, 759 w, and 517 m.

2.2. *X-ray structure determination*

All data collections were carried out on a Siemens P4 diffractometer employing a graphite monochromator. The structures were solved by direct methods using SHELXS-97 [9] and refined on F^2 using SHELXL-97 [9]. Hydrogens bonded to carbon were placed in calculated positions and refined as a riding model with fixed isotropic U's. For **2**–**4**, hydrogens bonded to nitrogen were located in the difference map and their positions refined with fixed isotropic U's. For **1**, pyridinium hydrogens were located in the difference map and their positions refined with fixed isotropic U's while amino hydrogens were placed in calculated positions and refined as a riding model with fixed isotropic U's. Neutral scattering factors and anomalous dispersion corrections for non-hydrogen atoms were taken from Ibers and Hamilton [10]. All data reduction, structure solution and refinement, absorption corrections (*via* psi scans) and graphics were performed by using SHELXTL (VMS) software [11]. Full crystallographic data are given in table 1 along with selected bond lengths and angles in table 2.

2.3. *Magnetic data collection*

Samples for magnetic data collection were prepared by finely grinding single crystals into a powder and packing the powder into a #3 gelatin capsule. External field dependent magnetic susceptibilities were measured at 1.8 K in the range of 0–50,000 Oe. Several points were taken as the field was reduced back to zero to test for hysteresis. All four compounds showed higher magnetization during the downward sweep. Tests using samples mixed with a small amount of silicon grease showed that this effect could be eliminated, suggesting that it was induced by mechanical rearrangement of the powdered samples within the capsule at high field. No hysteresis was observed in samples packed with silicon grease to prevent such movement. Temperature-dependent magnetic susceptibilities were determined in a field of 1000 Oe and in the range of 1.8–310 K on a Quantum Design MPMS-XL SQUID magnetometer on samples cooled in zero field. Single-crystal magnetic data were collected on 28.2 mg of crystals of **1** with the applied field oriented in three perpendicular directions relative to the crystal. Corrections were made for the background, the temperature-independent paramagnetic contribution of the Cu ion, and diamagnetic contributions of the samples according to Pascal's constants (**1** and **2**, -0.000339; **3** and **4**, -0.000398 emu Oe-mol^{-1}).

3. Results

3.1. *Syntheses*

The reaction of one equivalent of metal halide with two equivalents of the organic base in aqueous acid gave the desired salts as blue plates of $(3\text{-MAPH})_2CoBr_4$ (**1**),

Table 1. Crystallographic data for **1**–**4**.

Compound	**1**	**2**	**3**	**4**
Empirical formula	$C_{12}H_{18}Br_4CoN_4$	$C_{12}H_{18}Br_4CoN_4$	$C_{12}H_{20}Cl_4CoN_4O$	$C_{12}H_{18}Cl_4CoN_4$
Formula weight	596.87	596.87	437.05	419.03
Temperature (K)	163(2)	158(2)	158(2)	150(2)
Wavelength (Å)	0.71073	0.71073	0.71073	0.71073
Crystal system	Triclinic	Monoclinic	Triclinic	Monoclinic
Space group	$P\bar{1}$	$P2_1/n$	$P\bar{1}$	$P2_1/c$
Unit cell dimensions (Å, °)				
a	7.600(5)	8.473(2)	7.1117(7)	8.079(2)
b	9.231(3)	14.785(3)	8.6909(9)	14.667(6)
c	14.554(11)	15.674(3)	16.5315(17)	15.705(4)
α	89.11(4)	90	82.7210(10)	90
β	89.14(7)	103.293(11)	78.7730(10)	103.11(2)
γ	67.47(3)	90	69.3550(10)	90
Volume (Å^3), Z	943.0(10), 2	1911.0(7), 4	935.97(16), 2	1812.5(10), 4
Calculated density (mg m^{-3})	2.102	2.075	1.551	1.536
F(000)	570	1140	446	852
Crystal size (mm^3)	$0.75 \times 0.45 \times 0.30$	$0.84 \times 0.62 \times 0.28$	$0.73 \times 0.39 \times 0.08$	$0.80 \times 0.60 \times 0.30$
Reflections collected	3317	2897	8314	3731
Independent reflection	3288	2470	3593	2370
Max. and min. transmission	0.1651 and 0.0538	0.8149 and 0.1912	1.0000 and 0.7342	0.361 and 0.213
Parameters	198	210	223	210
Goodness-of-fit on F^2	0.949	0.951	1.034	1.032
Final R indices [$I > 2\sigma(I)$]	$R_1 = 0.0506$, $wR_2 = 0.1225$	$R_1 = 0.0383$, $wR_2 = 0.0873$	$R_1 = 0.0230$, $wR_2 = 0.0601$	$R_1 = 0.0331$, $wR_2 = 0.0812$

Table 2. Selected bond lengths (Å) and angles (°) for **1**–**4**.

		1	**2**	**3**	**4**
Bond lengths	Co–X(1)	2.4085(18)	2.3823(17)	2.2922(5)	2.2472(11)
	Co–X(2)	2.4103(18)	2.3964(17)	2.2727(5)	2.2641(10)
	Co–X(3)	2.403(2)	2.4230(17)	2.2646(5)	2.2975(10)
	Co–X(4)	2.410(2)	2.4260(17)	2.2760(5)	2.2931(11)
Bond angles	X(1)–Co–X(2)	110.76(7)	113.43(7)	110.245(17)	113.78(4)
	X(1)–Co–X(3)	108.44(7)	107.50(6)	109.847(18)	108.98(4)
	X(1)–Co–X(4)	106.82(7)	113.22(6)	103.608(19)	111.60(4)
	X(2)–Co–X(3)	105.00(7)	110.64(6)	108.110(17)	109.04(4)
	X(2)–Co–X(4)	111.67(7)	104.93(6)	111.468(18)	105.29(4)
	X(3)–Co–X(4)	114.17(8)	106.97(7)	113.510(18)	107.96(4)

(5-MAPH)$_2$CoBr$_4$ (**2**), (3-MAPH)$_2$CoCl$_4$(H$_2$O) (**3**), and blue cubes of (5-MAPH)$_2$CoCl$_4$ (**4**) in yields ranging from 26% to 76% (scheme 1). Crystals suitable for X-ray crystallography were grown through slow evaporation.

3.2. *Structure analysis*

3.2.1. (3-MAPH)$_2$CoBr$_4$ (1). Compound **1** crystallizes in the triclinic space group $P\bar{1}$. The asymmetric unit is shown in figure 1 and the selected bond lengths and angles are given in table 2. The $CoBr_4^{2-}$ forms as nearly ideal tetrahedra with $<5\%$ distortion

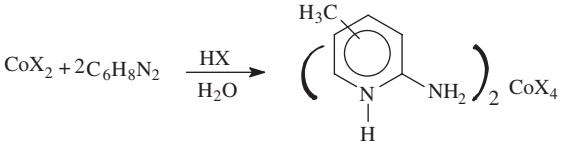

Scheme 1. Preparation of compounds **1**–**4**.

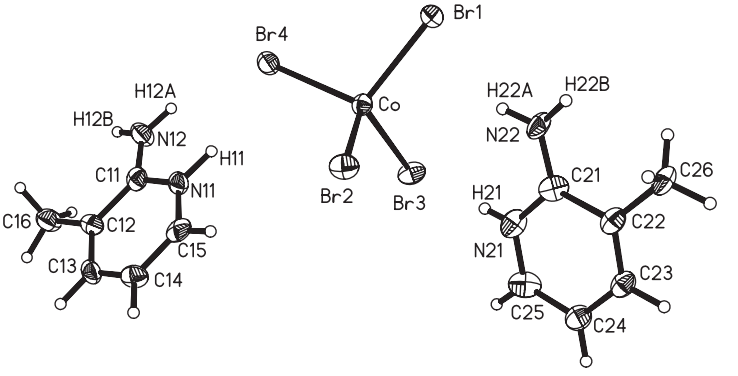

Figure 1. A thermal ellipsoid plot of the asymmetric unit of **1**. H-atoms are shown as spheres of arbitrary size. Only those H-atoms involved in hydrogen bonding are labeled.

from 109.5° for all angles around the metal and an average Co–Br bond length of 2.408(3) Å. The $CoBr_4^{2-}$ anions form chains parallel to the *a*-axis (figures 2 and 3) *via* long halide–halide contacts between translation-related units (Br4 · · · Br3B and Br3 · · · Br4C = 4.635(2) Å). The Co–Br4 · · · Br3B bond angle is 103.4(1)° while the CoB–Br3B · · · Br4 angle is 131.5(1)°, with a Co–Br4 · · · Br3B–Co torsion angle of 110.5(1)°. The chains are further linked antiparallel to one another *via* short contacts between inversion-related tetrabromocobaltates giving an overall ladder structure. The halide–halide contacts that make up the rungs of the ladder have a Br4 · · · Br4A distance of 4.234(3) Å with a Co–Br · · · Br bond angle of 100.0(1)°. The rungs form with a Co–Br · · · Br–Co torsion angle of 180° as required by symmetry.

The 3-MAP cations have alternating orientation with respect to the *ac*-plane, either parallel or perpendicular. Within any given stack of 3-MAPH cations, adjacent ions are related by inversion resulting in an alternation of orientation down each stack. The structure is stabilized by hydrogen bonds between the amino and pyridinium protons and bromide (table 3).

3.2.2. $(5\text{-MAPH})_2CoBr_4$ (2). Compound **2** crystallizes in the monoclinic space group $P2_1/n$. $CoBr_4^{2-}$ is again nearly an idealized tetrahedron (figure 4), with an average Co–Br bond length of 2.406(3) Å. The short contacts between bromides in adjacent anions form chains (Br2 · · · Br4A = Br4 · · · Br2B = 4.148(2) Å). The chains are connected to one another *via* pairwise contacts between Br3 · · · Br4A along with Br4 · · · Br3A = 4.278(2) Å. These bi-linked chains form a honeycomb-like structure (figure 5). The 5-MAPH cations are arranged in two fashions, either parallel or perpendicular to the *ac*-plane. Adjacent cations are related by an inversion center,

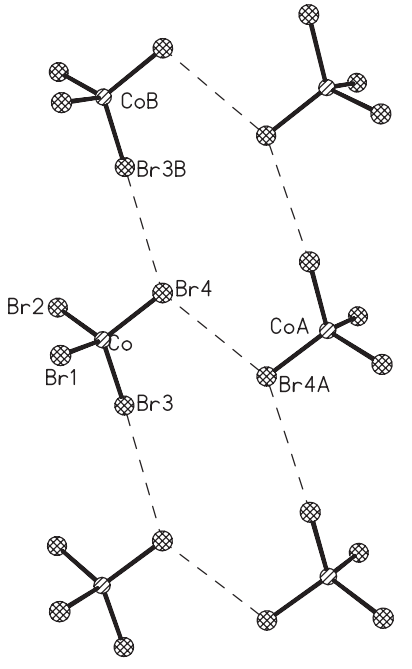

Figure 2. The short bromide $\cdots$ bromide contacts between $CoBr_4^{-2}$ ions in **1** form ladders. The rails of the ladder are formed by unit cell translations of $CoBr_4^{-2}$ while the rungs are formed by inversion-related ions.

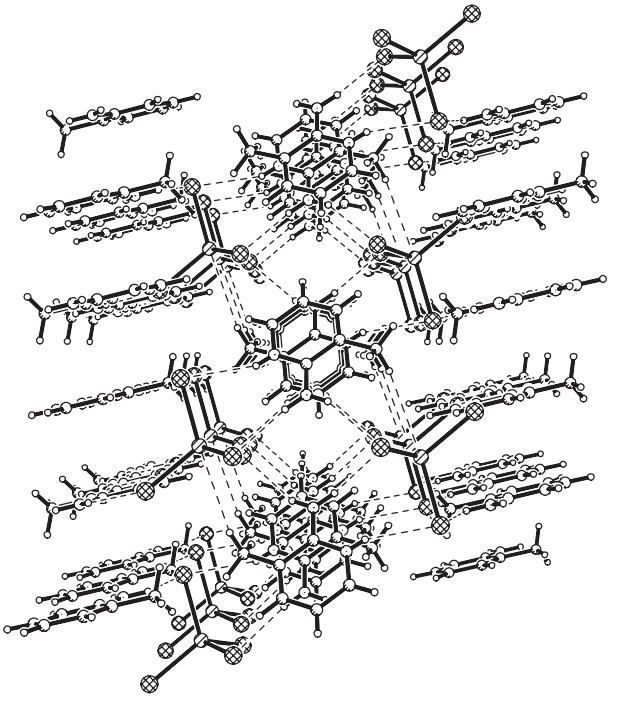

Figure 3. The crystal structure of **1** viewed parallel to the *a*-axis. Dashed lines show hydrogen bonds and short bromide $\cdots$ bromide contacts.

Table 3. Hydrogen bonds in **1**.

D–H···A	*d*(D–H)	*d*(H···A)	*d*(D···A)	∠(DHA)
N(11)–H(11)···Br(4)	0.99(9)	2.37(10)	3.318(8)	159(7)
N(12)–H(12A)···Br(4)	0.88	2.66	3.453(8)	151.1
N(21)–H(21)···Br(3)	0.75(10)	2.69(10)	3.399(8)	158(10)
N(22)–H(22A)···Br(1)	0.88	2.7	3.515(8)	154.9
N(22)–H(22B)···Br(2)$^{\#1}$	0.88	2.68	3.520(8)	159

Symmetry code: $^{\#1}-x, -y, -z+1$.

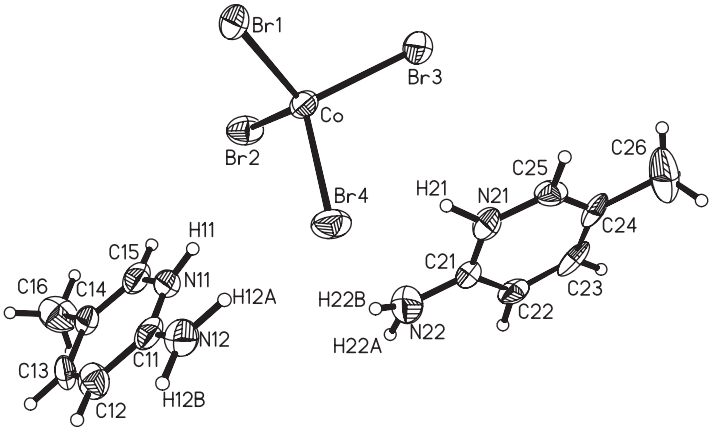

Figure 4. A thermal ellipsoid plot of the asymmetric unit of **2**. H-atoms are shown as spheres of arbitrary size and only those hydrogens whose positions were refined are labeled.

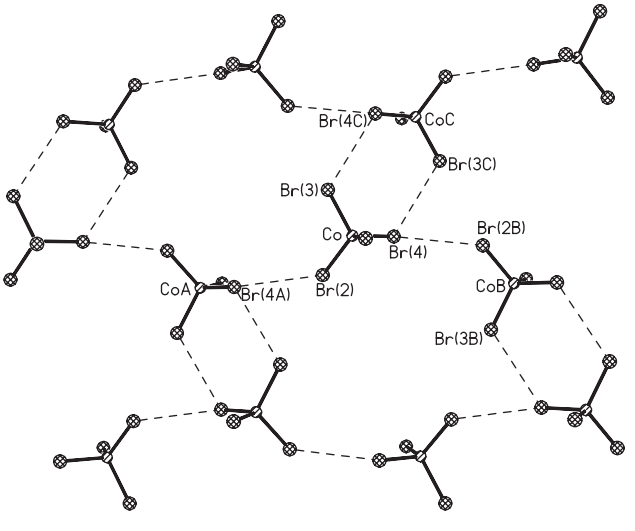

Figure 5. The close contacts observed in **2** and **4** create a honeycomb-like structure. The dashed lines show short Br···Br contacts between adjacent anions.

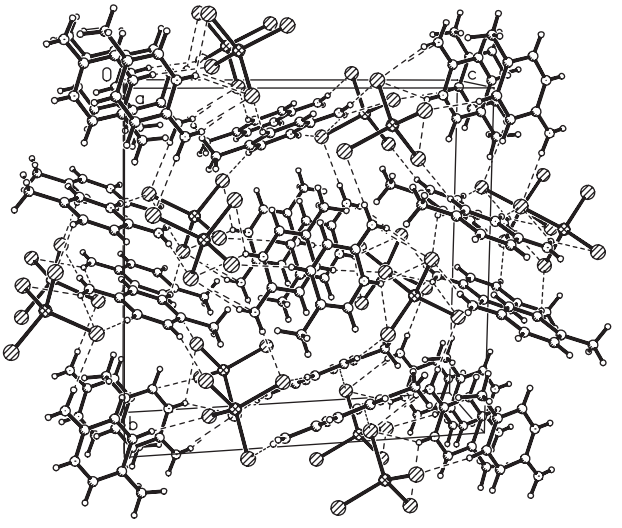

Figure 6. The crystal structure of **2** viewed parallel to the *a*-axis. Dashed lines show hydrogen bonds and short bromide···bromide contacts.

alternating the orientation of the two nitrogens (figure 6). The cations are held in the center of the voids within the honeycomb layers by hydrogen bonds from amino hydrogens to bromides (table 4).

3.2.3. (3-MAPH)$_2$CoCl$_4$(H$_2$O) (3). Compound **3** crystallizes in the triclinic space group $P\bar{1}$. The $CoCl_4^{2-}$ ions have average Co–Cl bond length of 2.276(3) Å and the halides form a near-ideal tetrahedron around the metal, with the exception of the angles related to Cl(4) [103.6(2), 111.5(2), and 113.5(2)°]. Halide–halide contacts form chains that are parallel to the *a*-axis due to contacts between Cl3A···Cl1B 4.119(2) Å. The presence of a water in the unit cell (figure 7) stabilizes the chains through hydrogen bonds to Cl2A and Cl1B (O–Cl = 2.469(2) and 2.844(2) Å, respectively, (figure 8). The CoA–Cl3A···Cl1B bond angle is 136.4(1)° and the CoB–Cl1B···Cl3B bond angle is 109.1(1)°. The resulting torsion angle of CoA–Cl3A···Cl1B–CoB is −99.0(2)°. The 3-MAP cations lie parallel to the *bc*-plane and are stacked parallel to the *a*-axis (figure 9). Hydrogen bonding occurs between the pyridinium hydrogens and the amine nitrogen with chlorides as well as an additional contact between a hydrogen on the amino nitrogen and oxygen in water (table 5).

3.2.4. (5-MAPH)$_2$CoCl$_4$ (4). Compound **4** crystallizes in the monoclinic space group $P2_1/c$ and is nearly isostructural with **2**. The $CoCl_4^{2-}$ retains its nearly ideal tetrahedral geometry and has an average Co–Cl bond length of 2.275(1) Å. The short contacts that form the chains Cl2···Cl4A and Cl4···Cl2B are 4.205(2) Å. The chain angles Co–Cl4···Cl2B and CoB–Cl2B···Cl4 form as 133.5(1)° and 133.3(1)°, respectively, with a corresponding torsion angle Co–Cl4···Cl2B–CoB of 115.8(2)°. Contacts between Cl3···Cl4C and Cl4···Cl3C are 4.349(2) Å. The double bridge shows angles Co–Cl3···Cl4C = 122.8(1)° and CoC–Cl4C···Cl3 = 120.3(1)°, with a Co–Cl3···Cl4C–CoC torsion angle of 36.7(1)°. Hydrogen bond parameters are given in table 6.

Table 4. Hydrogen bonds in **2**.

D–H···A	*d*(D–H)	*D*(H···A)	*d*(D···A)	∠(DHA)
N(12)–H(12A)···Br(4)	1.05(10)	2.35(10)	3.382(10)	167(8)
N(12)–H(12B)···Br(3)$^{\#1}$	1.09(10)	2.40(10)	3.434(10)	159(8)

Symmetry code: #1: $-x+1, -y, -z$.

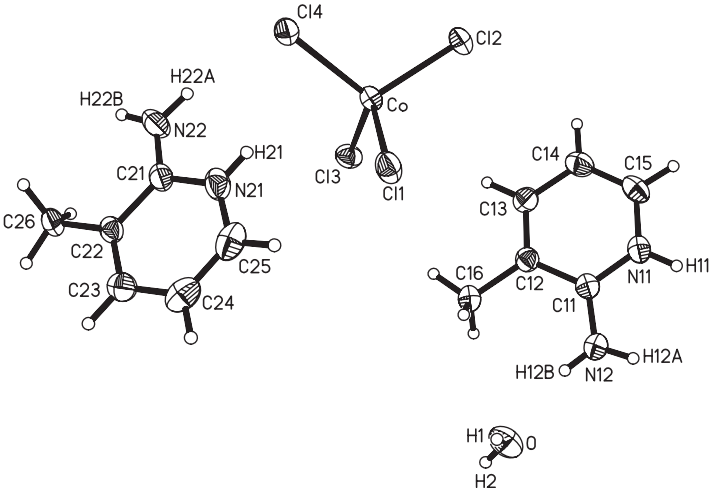

Figure 7. A thermal ellipsoid plot of the asymmetric unit of **3**. Hydrogens are shown as spheres of arbitrary size and only those whose positions were refined are labeled.

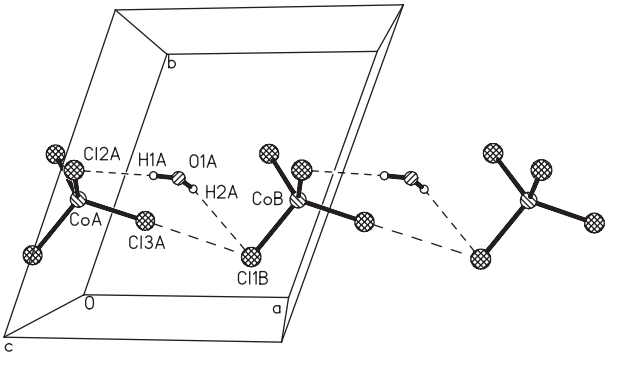

Figure 8. The short contacts between Cl^- on neighboring anions and the hydrogen bonding occurring with water form chains parallel to the *a*-axis.

3.3. *Magnetic data*

Magnetic susceptibility data were collected from 1.8 to 310 K for **1**–**4** in a 1 kOe applied field. A plot of χ_T *versus* T is shown in figure 10. The differing slopes at low temperature and the differing temperatures at which the decrease in moment is apparent suggest differing involvement of single-ion anisotropy, antiferromagnetic interactions, or both.

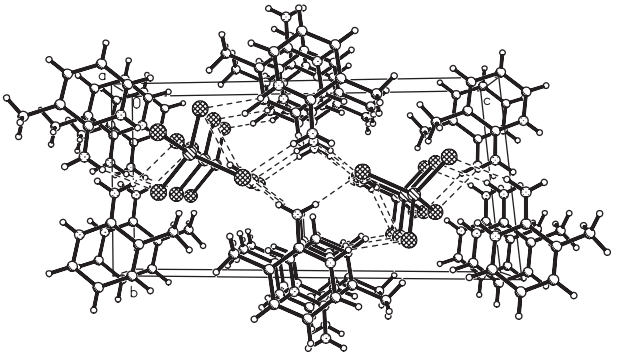

Figure 9. The crystal structure of **3** viewed parallel to the *a*-axis. Dashed lines show hydrogen bonds and short chloride···chloride contacts.

Table 5. Hydrogen bonds in **3**.

D–H···A	*d*(D–H)	*d*(H···A)	*d*(D···A)	∠(DHA)
N(11)–H(11)···Cl(1)$^{\#3}$	0.85(2)	2.37(2)	3.1495(15)	152.8(18)
N(12)–H(12A)···Cl(2)$^{\#3}$	0.82(2)	2.56(2)	3.3571(16)	163.7(19)
N(22)–H(22B)···Cl(3)$^{\#4}$	0.84(2)	2.49(2)	3.2969(18)	162(2)
N(12)–H(12B)···O	0.84(2)	2.05(2)	2.861(2)	164(2)
N(21)–H(21)···Cl(1)	0.83(2)	2.81(2)	3.3742(15)	126.3(17)
N(21)–H(21)···Cl(4)	0.83(2)	3.00(2)	3.6925(17)	142.2(18)
N(22)–H(22A)···Cl(4)	0.87(2)	2.37(2)	3.2315(17)	167(2)
O(1)–H(1)···Cl(2)$^{\#1}$	0.82(2)	2.47(3)	3.2765(17)	168(2)
O(1)–H(2)···Cl(1)$^{\#2}$	0.69(2)	2.84(2)	3.4732(16)	153(3)

Symmetry code: #1: x, $y-1$, z; #2: $x+1$, $y-1$, z; #3: $-x+2$, $-y$, $-z+1$; #4: $-x+2$, $-y+1$, $-z$.

Table 6. Hydrogen bonds in **4**.

D–H···A	*d*(D–H)	*D*(H···A)	*d*(D···A)	∠(DHA)
N(11)–H(11)···Cl(3)$^{\#1}$	0.90(4)	2.31(4)	3.216(3)	175(3)
N(12)–H(12B)···Cl(4)$^{\#2}$	0.80(4)	2.52(4)	3.312(4)	168(4)
N(22)–H(22A)···Cl(4)$^{\#3}$	0.76(4)	2.52(4)	3.239(4)	158(4)
N(22)–H(22B)···Cl(3)	0.89(4)	2.41(4)	3.303(4)	178(4)

Symmetry code: #1: $-x+1$, $-y+1$, $-z$; #2: $-x$, $-y+1$, $-z$; #3: $-x$, $y-0.5$, $-z+0.5$.

The susceptibility data for **2**–**4** were fit to a model for single-ion anisotropy with a Curie–Weiss correction for antiferromagnetic interactions and to the model for a uniform $S=3/2$ chain. The data and fits are shown in figure 11 and the parameters resulting from the best-fit models are given in table 7. No maxima in χ are observed in any of the compounds which reach maximum values at 1.8 K of **2** = 1.09, **3** = 0.43, and **4** = 0.76 emu mol^{-1}. In all cases, the best fits were obtained using the single-ion anisotropy model.

Compound **1** shows an increasing χ value as the temperature decreases, reaching a maximum of 1.59 emu mol^{-1} at 1.8 K. The χ_T *versus* T_{plot} shows a relatively constant value between 100 and 300 K, but then begins to rise as temperature decreases further to a maximum of 3.82 emu-K mol^{-1} at 7.9 K (figure 12).

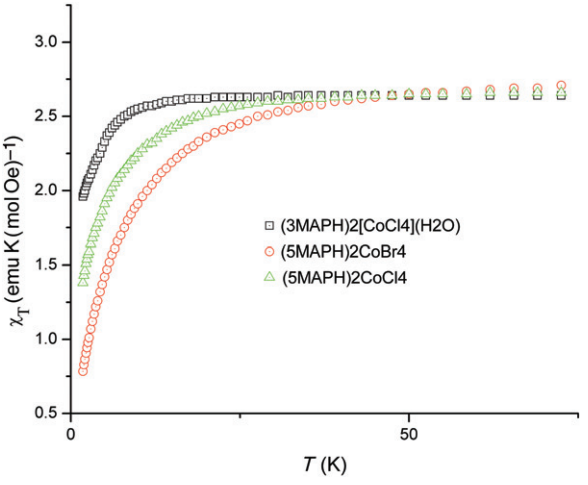

Figure 10. A plot of χ_T *vs.* T for **2**–**4**.

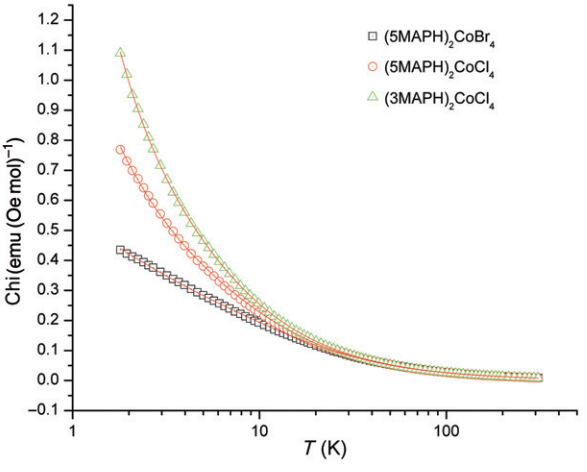

Figure 11. A plot of χ_T *vs.* log T for **2**–**4**. The solid lines show the fits to the single-ion anisotropy model with a Curie–Weiss correction for antiferromagnetic interactions.

Table 7. Fitted magnetic parameters for **2**–**4**.

Compound	C (emu K (mol Oe)$^{-1}$)	θ (K)	D (K)
(5-MAPH)$_2$CoBr$_4$ (**2**)	2.72(1)	−1.75(1)	−24.1(3)
	2.86(1)	−4.90(3)	N/A
(3-MAPH)$_2$[CoCl$_4$](H$_2$O) (**3**)	2.643(4)	0.229(2)	−11.9(1)
	2.65(1)	−0.69(1)	N/A
(5-MAPH)$_2$CoCl$_4$ (**4**)	2.59(1)	−0.215(7)	−17.1(3)
	2.58(1)	−1.63(2)	N/A

C, Curie constant; θ, Weiss constant; and D, single-ion anisotropy. The first row for each compound includes a single ion anisotropy term in the model while the second does not.

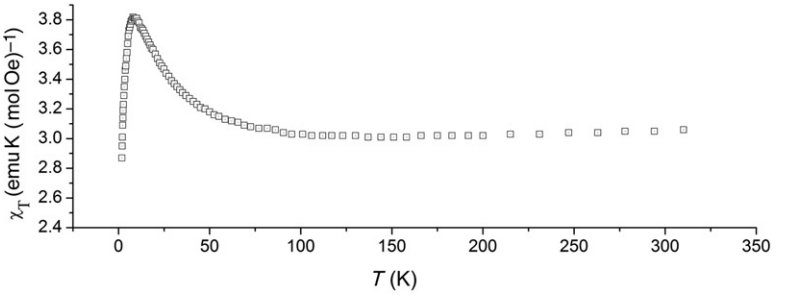

Figure 12. The χ_T *vs.* T powder data for **1**.

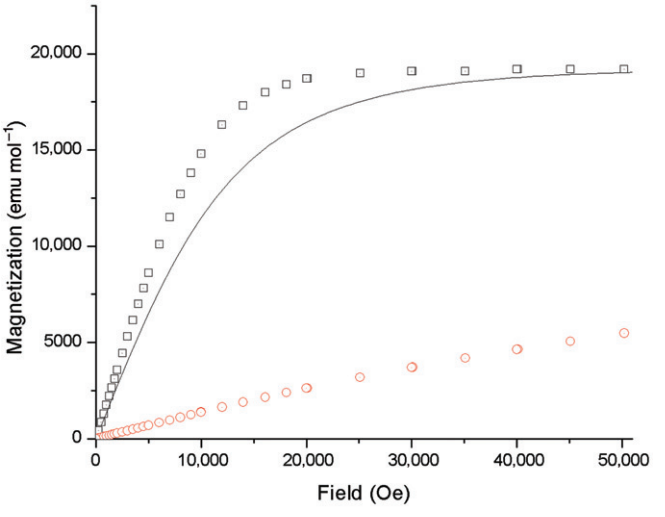

Figure 13. The single-crystal molar magnetization of **1** at 1.8 K is shown as a function of field up to 50 kOe for several orientations. The circles represent M_{mol} when the field is applied normal to the plates (parallel to the c-axis); the squares represent M_{mol} when the field lies within the plates. (Measurements in two orthogonal directions within the plates were indistinguishable). The solid line corresponds to $S = 3/2$ Brillouin function with a g-factor of 2.4.

This observed rise is in the χ_T plot suggests ferromagnetic interactions, while the sudden drop as the temperature decreases from 7.9 to 1.8 K suggests either antiferromagnetic interactions or a loss in moment due to single-ion effects as seen in **2**–**4**.

Attempts to fit the data observed for powdered samples of **1** were unsuccessful against a variety of available models, so single-crystal data were collected on a single crystal (thin plate) and compared to the expectation for a paramagnetic $S = 3/2$ system. When the field is applied perpendicular to the plate (parallel to the c-axis), the resulting data are lower than the predicted paramagnetic curve (figure 13, lower curve). When the field is applied parallel to the plate, the observed magnetism is greater than the paramagnetic model (figure 13, upper curve).

4. Discussion

4.1. *Synthesis and structure analysis*

The four products showed varying shades of blue with the two Cl compounds a very similar navy blue and the two Br compounds a somewhat lighter blue. Only **3** crystallized as a hydrate. The syntheses of **1**–**4** were straightforward and good sized single crystals could be recovered. The presence of an excess of acid in solution was essential to keep the Co(II) ions from binding to the pyridine ring.

The structures of the cations are similar to previously published 3-MAPH and 5-MAPH salts with comparable bond angles and lengths [12–14]. The same type of stacking with alternating orientation of the cations was observed in all four compounds, and has also been observed in the previously published work. For these complexes, we suggest that not surprisingly, it is the size and shape of cation that influences the packing, and hence the space group, of each compound. This is strongly supported by the observation that both 3-MAPH salts crystallize in $P\bar{1}$ while the 5-MAPH salts crystallize in the closely related space groups $P2_1/n$ and $P2_1/c$. A possible explanation for this is the difference in location of the methyl group. The 3-MAPH has its bulk directed to one side of the molecule as a result of the 2,3-substitution. In the $P\bar{1}$ space group, the 3-MAPH ions are related by the inversion center which allows an even distribution of the substituents and minimizes potential voids in the crystal. The 5-MAPH has a more evenly distributed volume as a result of the methyl and amino groups being *para* to one another. In the monoclinic state, the cations pack such that the methyl and amino groups alternate position, reducing the overall dipole moment of the system. Within each halide, the Co–X bond lengths vary little. The geometry about cobalt is nearly tetrahedral in all four compounds, as expected for four-coordinate cobalt(II) [15]. The presence of water in **3** and the resulting hydrogen bonds prevent the ladder formation seen in **1**. As expected, **2** and **4** show nearly identical structures, with the close halide$\cdots$halide contacts forming a honeycomb layer structure and the cations locate in the centers of the voids in the layers in both complexes.

4.2. *Magnetic data*

Compounds **2**–**4** were compared against a uniform spin, $S = 3/2$, chain model as well as a model for single-ion anisotropy with a Curie–Weiss correction for antiferromagnetic interactions. Compounds **2**–**4** have varying degrees of single-ion anisotropy and antiferromagnetic interactions, which can be seen by the y-intercept of their respective χ_T *versus* T curves (figure 11). The low-temperature limit for χ_T in such cases is 1.7 when there are no internal interactions, while compounds that also exhibit antiferromagnetic exchange will decrease below that value at low temperatures [16]. It is clear from figure 11 that **2** exhibits predominately single-ion anisotropy, while **3** is dominated by antiferromagnetic interactions (χ_T approaches 0.5 at 1.8 K). An intermediate case is observed with **4**, where the χ_T approaches a value of $\sim$1.25 at 1.8 K, implying comparable contributions from both single-ion anisotropy and weak antiferromagnetic interactions.

Compound **1** behaves significantly different from **2**–**4**. In contrast to the steady decrease of χ_T at low temperatures found for those compounds (figure 10), χ_T for **1**, constant between 300 and 100 K, increases by nearly 20% between 100 and 8 K, reaching a maximum of 3.82 emu-K (mol-Oe)$^{-1}$ at 7.9 K before dropping sharply at lower temperatures (figure 12).

One possible explanation for the behavior of **1** would be a change of sign of the single-ion anisotropy parameter. Negative values of D found for the other three compounds correspond to $m_S = \pm 1/2$ substrates lying an energy D below the $m_S = \pm 3/2$ substrates; as the higher level states corresponding to larger moments are vacated upon cooling, the effective moment of the ion decreases. Under this condition, the Co(II) would have an easy-plane anisotropy. On the other hand, with the $m_S = \pm 3/2$ substates low, the opposite behavior occurs and the effective moment is predicted to grow upon cooling and to reach a higher constant value as T approaches zero. The ion would then have a strong easy-axis anisotropy. The observed decrease of χ_T below 7.9 K could be due to the presence of weak antiferromagnetic interactions between the $CoBr_4$ dianions.

The single-crystal magnetization of **1** at 1.8 K (figure 13) clearly shows easy-plane behavior. When the field is applied within the crystal plane, the molar magnetization reaches a saturation value near 18,800 emu mol^{-1} by 30 kOe. Essentially identical behavior is found for different directions within the plane. In contrast, the molar magnetization with the field normal to the plane is less than one-third of the saturation value at 50 kOe and still increasing linearly. Easy-plane behavior corresponds to a negative D value, as found for **2**–**4**. Given the strong structural similarities of the $CoBr_4^{2+}$ coordination spheres, this conclusion is not surprising.

The upturn in χ_T of **1** below 100 K can then be attributed to the presence of a ferromagnetic interaction which is sufficiently strong to overcome the intrinsic decrease in moment caused by the negative D-value. It is reasonable to attribute the source of this interaction to the shorter (4.23 Å) Br4 · · · Br4A interaction between inversion-related tetrabromocobaltates (figure 2); this interaction would lead to formation of ferromagnetic dimers in **1**. However, such dimers are linked into structural ladders by the longer (4.64 Å) Br4 · · · Br3B and Br3 · · · Br4C contacts between translation-related units (figure 3). If this linkage were weaker and antiferromagnetic, it could account for the decrease in χ_T below 7.9 K.

Isolated spin ladders [17] are known to have cooperative singlet-ground states with an energy gap Δ between the ground state and higher states with magnetic moments; these gaps cause the spin-ladder susceptibilities to reach a maximum at a temperature dependent on the dominant antiferromagnetic interaction and then to decrease exponentially to zero at lower temperatures. The magnetization of a spin ladder decreases exponentially with decreasing temperature for $T < \Delta$. In the $T = 0$ limit, it remains zero until the external field is large enough to close the gap through Zeeman splitting. The large magnetization observed at 1.8 K for **1** (figure 13) is consistent with the spin-ladder model provided $\Delta \ll 1.8$ K. Experiments at lower temperatures are necessary to test the validity of this model.

The difference of magnetic interactions observed between **2** and **4** despite their similar structures is due to the limiting size of the 5-MAP. The large size of the cation prevents the $CuCl_4^{2-}$ ions from compensating completely for the reduction in the size of the smaller halide, resulting in a smaller orbital overlap and hence weaker magnetic interactions.

The influence of the water molecule in **3** is likely the principle cause for the differences in magnetic behavior between **1** and **3**. Hydrogen bonding between water and $CuCl_4^{2-}$ results in shorter $X \cdots X$ distances within the chain, but the bulk of the water forces the tetrachlorocobaltate ions further apart perpendicular to the chains, disrupting the ladder structure observed in **1**.

5. Conclusions

A family of tetrahalocobaltate salts has been prepared and analyzed *via* X-ray diffraction and variable temperature magnetic susceptibility. Three of the complexes exhibit a combination of weak single-ion anisotropy and weak antiferromagnetic interactions while the fourth, $(3\text{-MAPH})_2CoBr_4$ (**1**), shows evidence of both stronger ferromagnetic and weaker antiferromagnetic interaction, as well as the presence of an easy-plane anisotropy. A spin-ladder model is proposed which will require additional low-temperature experiments to verify.

Acknowledgments

Financial assistance from the National Science Foundation (NSF) (IMR-0314773), the Kresge Foundation, and PCI Synthesis toward the purchase of the MPMS SQUID magnetometer and powder diffractometer are gratefully acknowledged.

References

[1] (a) K. Halvorson, R.D. Willett. *Acta Cryst.*, **C44**, 2071 (1988); (b) G.V. Rubenacker, J.E. Drumheller. *J. Magn. Magn. Mater.*, **79**, 119 (1989); (c) P. Zhou, J.E. Drumheller. *J. Appl. Phys.*, **67**, 5755 (1990).
[2] H. Place, R.D. Willett. *Acta Cryst.*, **C43**, 1050 (1987).
[3] A.R. Parent, C.P. Landee, M.M. Turnbull. *Inorg. Chim. Acta*, **360**, 1943 (2007).
[4] (a) T. Manfredini, G.C. Pellacani, A. Bonamartini-Corradi, L.P. Battaglia, G.G.T. Gaurini, J.G. Guisti, R.D. Willett, D.X. West. *Inorg. Chem.*, **29**, 221 (1990); (b) C. Zanchini, R.D. Willett. *Inorg. Chem.*, **29**, 3027 (1990).
[5] M.M. Turnbull, C.P. Landee, B.M. Wells. *Coord. Chem. Rev.*, **249**, 2567 (2005) and references therein.
[6] (a) T.E. Grigereit, B.L. Ramakrishna, H. Place, R.D. Willett, G.C. Pellacani, T. Manfredini, L. Menabue, A. Bonamartini, L.P. Battaglia. *Inorg. Chem.*, **26**, 2235 (1987); (b) H. Place, R.D. Willett. *Acta Crystallogr., Sect. C*, **43**, 1497 (1987).
[7] T. Coffey, C. Landee, W. Robinson, M. Turnbull, M. Winn, F. Woodward. *Inorg. Chim. Acta*, **303**, 54 (2000).
[8] (a) R. Al-Far, B.F. Ali, K. Al-Sou'oud. *J. Chem. Crystallogr.*, **36**, 523 (2006); (b) A.S. Albrecht, C.P. Landee, M.M. Turnbull. *J. Chem. Crystallogr.*, **33**, 269 (2003); (c) R. Al-Far, B.F. Ali. *J. Chem. Crystallogr.*, **38**, 373 (2008).
[9] (a) G.M. Sheldrick. *SHELXS-97, Program for the Solution of Crystal Structures*, University of Gottingen, Gottingen, Germany (1997); (b) G.M. Sheldrick. *SHELXL-97, Program for the Refinement of Crystal Structures*, University of Gottingen, Gottingen, Germany (1997).
[10] J.A. Ibers, W.C. Hamilton (Eds.). *International Tables for Crystallography*, Vol. C, Kynoch Press, Birmingham (1992).
[11] *SHELXTL/PC*, Siemens Corp., Madison, WI (1990).

[12] T.J. Coffey, C.P. Landee, W.T. Robinson, M.M. Turnbull, M. Winn, F.M. Woodward. *Inorg. Chim. Acta*, **303**, 54 (2000).
[13] R. Al-Far, B.F. Ali, K. Al-Sou'oud. *J. Chem. Crystallogr.*, **36**, 523 (2006).
[14] F.M. Woodward, C.P. Landee, J. Giantsidis, M.M. Turnbull, C. Richardson. *Inorg. Chim. Acta*, **324**, 324 (2001).
[15] C.W. Yeh, H.L. Hu, R.H. Liang, K.M. Wang, T.Y. Yen, J.D. Chen, J.C. Wang. *Polyhedron*, **24**, 539 (2005).
[16] O. Kahn. *Molecular Magnetism*, Wiley-VHC Inc, New York (1993).
[17] (a) E. Dagotto, J. Riera, D.J. Scalapino. *Phys. Rev. B*, **45**, 5744 (1992); (b) E. Dagotto. *Rev. Mod. Phys.*, **66**, 763 (1994); (c) E. Dagotto, T.M. Rice. *Science*, **271**, 618 (1996).